MILLIMETER WAVE RADAR SCATTERING FROM CLOUD ICE CRYSTALS

Kültegin Aydın* and Thomas M. Walsh
Pennsylvania State University, University Park, PA, USA

1. INTRODUCTION

The growing interest in the use of millimeter wavelength radars for remote sensing of clouds requires a good understanding of the scattering characteristics of cloud ice crystals. This paper reviews some recent computational results on ice crystal scattering at 35, 94, and 220 GHz frequencies. Dual frequency ratios of reflectivity factors as function of size are presented. Polarimetric scattering signatures for differentiating and identifying ice crystal types are discussed for radar applications. Measurements with the University of Wyoming's airborne 95 GHz radar together with simultaneously obtained two-dimensional particle probe data are used to demonstrate some of these radar signatures.

2. ICE CRYSTAL MODELS

Fig. 1 shows the seven ice crystal models considered in this study. These can be grouped as "columnar" (hexagonal column), "planar" (hexagonal plate, stellar, and 4-90 bullet rosette), and "spatial" (4-109, 6-90, and 8-70 bullet rosettes). The 4-90 rosette is composed of four orthogonal bullets on the same plane. The 6-90 rosette has two additional bullets that are orthogonal to the plane of the 4-90 rosette. The 8-70 consists of two 4-90 rosettes whose planes intersect at an angle of 70^0. The 4-109 rosette is composed of four bullets attached at the center of a regular tetrahedron at 109^0 and extend out to its vertices. The dimensional relationships for the hexagonal column, hexagonal plate, stellar crystals, and the individual bullets in the bullet rosettes were obtained from published experimental observations (Auer and Veal 1970; Heymsfield 1972). The size of each crystal type is denoted by its maximum dimension D. For each rosette, D is twice the length of a single bullet, except for the 4-109 rosette. Since the 4-109 rosette has the same volume as the 4-90 rosette with identical bullets, its size D will also be denoted by twice the size of a single bullet, even though its maximum dimension is less than this. The density of all these crystals are assumed to be 0.9 g cm^{-3}. Lowering the density of the ice crystals does not change the trends presented in this paper, only the values of the parameters are changed. More detail on these models, as well as the effects of lowering the density, can be found in Walsh (1998) and Aydin and Walsh (1999). The ice crystals are assumed to be aligned, on average, with their largest dimensions along the horizontal plane (similar to the form shown in Fig. 1) such that they expose the largest surface area to this plane. Their orientation on the horizontal plane is random and a Gaussian distribution with 0^0 mean and 5^0 standard deviation (10^0 and 20^0 are also considered) represents the angular deviations (canting angle) from the horizontal plane.

Corresponding author address: Kültegin Aydın, Department of Electrical Engineering, Penn State University, University Park, PA 16802, USA, E-mail: k-aydin@psu.edu, Tel: (814) 865 2355, Fax: (814) 863 8457

3. SCATTERING FROM ICE CRYSTALS

The scattering calculations were performed using the finite-difference time-domain (FDTD) method with the second order Liao absorbing boundary condition (Kunz and Luebbers 1993; Taflove 1995). The T-matrix method (Waterman 1969; Mishchenko et al. 1999) was used for sizes below 0.4 mm for columns, 0.2 mm for plates and stellar crystals, and 0.1 for the remaining crystal types.

The scattering parameters considered here are the backscattering cross sections at horizontal and vertical polarizations $\langle\sigma_{hh}\rangle$ and $\langle\sigma_{vv}\rangle$, the differential reflectivity

$$Z_{DR} = \langle\sigma_{hh}\rangle / \langle\sigma_{vv}\rangle \quad (1)$$

the linear depolarization ratios

$$LDR_h = \langle\sigma_{vh}\rangle / \langle\sigma_{hh}\rangle \quad (2)$$

and

$$LDR_v = \langle\sigma_{hv}\rangle / \langle\sigma_{vv}\rangle \quad (3)$$

the dual frequency ratio

$$DFR(f_1/f_2) = (f_2/f_1)^4 \, |K_2/K_1|^2 \langle\sigma_{hh}(f_1)\rangle / \langle\sigma_{hh}(f_2)\rangle \quad (4)$$

and the correlation between the copolarized scattering amplitudes

$$\rho_{hv} = |\langle S_{hh}^* S_{vv}\rangle| / [\langle |S_{hh}|^2\rangle \langle |S_{vv}|^2\rangle]^{1/2} \quad (5)$$

The first and second subscripts denote the polarizations of the scattered and incident waves, respectively, and the triangle brackets $<\bullet>$ indicate averaging over the orientation distribution. The frequency is denoted by f with $f_1 < f_2$, and $K = (n^2 - 1)/(n^2 + 2)$, where n is the index of refraction of ice; at the frequencies considered here $|K_1/K_2| \approx 1$. Also, since the cross-polarized backscattering cross sections σ_{vh} and σ_{hv} are equal for reciprocal media, the following relationship is valid (Aydin and Walsh 1999, Aydin 1999)

$$LDR_v = LDR_h \times Z_{DR}. \quad (6)$$

Fig. 2 shows scattering parameters at 35, 94, and 220 GHz for ice crystals with size D = 0.8 mm as a function of elevation angle α measured from the horizontal plane ($\alpha = 0^0$ and 90^0 correspond to side and vertical incidence cases, respectively). The canting angle has zero mean and 5^0 standard deviation. The variation in $<\sigma_{hh}>$ is negligible at 35 GHz because the crystals are much smaller than the wavelength (Rayleigh scattering regime). At 94 GHz the "planar" crystals exhibit noticeable changes from side to vertical incidence since the depth along the incident wave's propagation direction is much larger (and comparable to the wavelength at 95 GHz) at side incidence than that at vertical incidence. The changes observed at 220 GHz are even more significant because of the resonance scattering effects at this smaller wavelength. The variation in $<\sigma_{hh}>$ is significantly less than $<\sigma_{vv}>$ (not shown here) for planar (and columnar) crystals because the horizontal polarization is lined up with the maximum dimension of the crystals at all angles.

As expected, Z_{DR} has its maximum value at side incidence ($\alpha = 0^0$) because the aspect ratio of most of these crystals is greatest at side incidence. The "spatial" rosettes (4-109, 6-90, and 8-70) have aspect ratios close to unity and show very little variation with elevation angle at 35 and 94 GHz. Although these lower frequencies are not sensitive to the small variations in the aspect ratios, the 220 GHz frequency is. Z_{DR} converges to 1 (0 dB in the figure) at vertical incidence ($\alpha = 90^0$) as a result of the orientation model which assumes random orientation on the horizontal plane. Z_{DR} shows significant differences between "columnar", "planar" (plate, 4-90 rosette, and stellar crystal), and "spatial" crystals at side incidence. At 35 and 94 GHz Z_{DR} for "spatial" crystals is near 0 dB, for "planar" crystals it varies between 5 to 10 dB, while for the "columnar" crystal it is about 3 dB. These differences in Z_{DR} might be useful for differentiating the three categories of ice crystals assuming that they are not mixed with other crystal types.

At vertical incidence, in contrast with Z_{DR}, LDR_h and ρ_{hv} show large differences between columns and other crystal types. LDR_h is greater than –15 dB for columns and less than -35 dB for planar and spatial crystals (with the exception of the 4-109 rosette, which has a value of about –30 dB at 220 GHz). ρ_{hv} for columns is 8 to 14 % below that of the other crystals. Another interesting aspect of these two parameters is that LDR_h increases for columns and decreases for planar crystals as α increases. This trend in LDR_h was noted earlier based on prolate and oblate model particles (Vivekanandan et al. 1990; Matrosov 1991). It should also be noted that for the orientation model used in these calculations LDR_h is below –25 dB at 35 and 94 GHz for all crystal types other than the column. However, if the standard deviation of the canting angle were larger than 5^0, then LDR_h would be higher.

Fig.3 shows the dual-frequency ratio $DFR(f_1/f_2)$ corresponding to frequencies f_1 and f_2 = 35, 94, 220 GHz for all the ice crystal models. It is clear that the DFR(35/94) is the weakest among the three pairs of frequencies for sizes below 1.5 mm (2 mm for columns). DFRs are generally high at side incidence and are very low (less than 2 dB) at vertical incidence for all crystals except the 8-70 rosette. DFR is enhanced when the crystals are randomly oriented (3rd column in Fig. 3) with a uniform random distribution (over 0^0 to 90^0) for the canting angle, which is different than the Gaussian distribution considered so far.

4. SIMULATIONS

The ice crystal models described in Section 2 were used together with gamma model size distributions of the form: $N(D) = N_0 D^{\mu} \exp(-\Lambda D)$ in $mm^{-1}\ m^{-3}$ units to simulate radar observables. Here N_0, μ, and Λ are the parameters of the distribution and D is the crystal size. Over 2200 size distributions were generated based on information available in the literature (Downing et al. 1990; Heymsfield et al. 1990). The ranges for various parameters used in the simulations were as follows: ice crystal sizes from 0.03 to 2 mm, μ from 0 to 2, total ice crystal concentration from 0.001 to 50 L^{-1}, and ice water content from 0.001 to 1 g m^{-3}. The median volume diameter and the mode diameter (where the distribution reaches its peak) were limited to values below 1 mm and 0.5 mm, respectively.

The radar observables that will be discussed here are the effective reflectivity factor at horizontal polarization 10 $\log(Z_h)$ in dBZ units with Z_h in $mm^6\ m^{-3}$ units, the difference reflectivity 10 $\log(Z_{DP})$ in dBZ units with $Z_{DP} = |Z_h - Z_v|$ in $mm^6\ m^{-3}$ units, the differential reflectivity $Z_{DR} = 10 \log(Z_h/Z_v)$ in dB units, and the linear depolarization ratio $LDR_v = 10 \log(Z_{hv}/Z_{vv})$ in dB units. The reflectivity factors are related to the backscattering cross sections, e. g., $Z_h = [\lambda^4/(\pi^5 |K|^2)]\ N_T <\sigma_{hh}>$, where the triangular brackets

here indicate averaging over the size and orientation distributions, λ is the wavelength, N_T is the total number of particles per unit volume, and $|K|^2 = |(n^2 - 1)/(n^2 + 2)|^2 = 0.177$ with n being the complex index of refraction of ice.

Fig. 4 shows the simulated scatter plots for Z_h vs. Z_{DP}, Z_h vs. Z_{DR}, and Z_h vs. LDR_v at 94 GHz corresponding to three different standard deviations (5^0, 10^0, and 20^0) of the canting angle with zero mean; notice the significant effect on the ratio parameters (Z_{DR} and LDR_v) and the modest effects on Z_h and Z_{DP}. These plots will be compared with radar measurements and in situ particle probe data next.

5. MEASUREMENTS

The data shown in Fig. 5 was obtained on April 2, 1997 during the WYICE'97 winter-spring campaign in Laramie, Wyoming. The University of Wyoming's King Air aircraft was equipped with a 95 GHz radar system and two dimensional particle probes, which provided shadow images of ice crystals as the aircraft penetrated cirrus clouds. The particle images were obtained at an altitude of 2860 m and temperature $-9\ ^0C$. These shadow images correspond to columnar crystals. The radar data was simultaneously obtained at side incidence (looking out from the side of the aircraft). 100 data points from the four closest range gates (120 to 210 m range with 30 m range gate spacing) over two seconds are shown (the aircraft roll is about 0^0 and its air speed is about 100 m s^{-1}). A two-gate running average (cross track) and a 0.6 second along track running average is performed on the data. The scatter plots of (Z_h , Z_{DP}), (Z_h , Z_{DR}), and (Z_h , LDR_v) are also presented in Fig. 5. The solid line shown on the Z_h - Z_{DP} plane was obtained by fitting a curve to the simulated results in Fig. 4 (the dashed line is for stellar crystals). Note that the radar data is clustered around the solid curve indicating a very good match. The data on the Z_h - Z_{DR} and Z_h - LDR_v planes also compare well with the simulated results of Fig. 4. The clustering in the Z_h-Z_{DR} and Z_h - LDR_v planes compare best with simulations based on a standard deviation of the canting angle between 5^0 to 10^0 and 10^0 to 20^0, respectively. Results for stellar crystals (not shown here) show good agreement as well (Walsh and Aydin 1999). In fact there is case where the aircraft has a 40^0 roll and the clustering signatures in all these planes compare well with simulated data taking into account the elevation angle. All of these results involving the simulations and radar measurements are being prepared for a journal publication.

It should also be noted that in a mixture of columnar (or planar) crystals with aggregates, the Z_h-Z_{DP} relationship might be useful for separating their relative contributions to the reflectivity factor (Aydin and Walsh 1998; Walsh 1998). This assumes that the aggregates produce similar returns at horizontal and vertical polarizations, similar to spherical particles. If such aggregates are in the mixture, then Z_{DP} is not altered by their presence and can be used together with Z_h (which is affected by the presence of the aggregates) to separate the contribution of the aggregates to the measured Z_h.

6. SUMMARY AND DISCUSSION

Scattering characteristics of single "columnar" (hexagonal column), "planar" (hexagonal plate, stellar crystal, 4-90 bullet rosette), and "spatial" ice crystals (4-109, 6-90, and 8-70 bullet rosettes) were presented at 35, 94, and 220 GHz frequencies. It was noted that at side incidence and 35 and 94 GHz frequencies Z_{DR} was distinctly different for all three crystal types and that this might be useful for differentiating them. At vertical incidence it was shown that the linear depolarization ratio LDR (LDR_h or LDR_v) and the correlation coefficient ρ_{hv} could be used for identifying "columnar" crystals. The elevation angle dependence of LDR was shown to be very different for "columnar" and "planar" crystals, which could also be useful for differentiating them. Among the dual frequency ratios of reflectivity factors DFR(35/94) was the weakest compared to DFR(94/220) and DFR(35/220) for crystal sizes below 1.5 mm (2mm for columns). DFRs were generally high at side incidence and very low (less than 2 dB) at vertical incidence for all crystals except the 8-70 rosette. DFR was enhanced when the crystals were randomly oriented. Finally, radar observables were simulated at 94 GHz for hexagonal columns using gamma model drop size distributions. These compared very well with side incidence radar measurements of columnar crystals (as indicated by in situ particle probe images) in terms of their clustering behaviors on the Z_h - Z_{DP}, Z_h and Z_{DR}, and Z_h - LDR_v planes. It was also noted that similar comparisons were made corresponding to an elevation angle of 40^0 for stellar crystals.

6. ACKNOWLEDGMENTS

This research was supported in part by the National Science Foundation under grants ATM-922516 and ATM-9813512. The authors would like to thank Dr. R. Kelly, M. Wolde, and D. Leon of the University of Wyoming for providing the radar data, and for helpful discussions on the data.

7. REFERENCES

Auer, A. H., and D. L. Veal, 1970: The dimensions of ice crystals in natural clouds. *J. Atmos. Sci.*, **27**, 919-926.

Aydin, K., and T. M. Walsh, 1998: Separation of millimeter-wave radar reflectivities of aggregates and pristine ice crystals in a cloud. *Int. Geosci. Remote Sensing Symp.*, Seattle, WA, 440-442.

Aydin, K., and T. M. Walsh, 1999: Millimeter wave scattering from spatial and planar bullet rosettes. *IEEE Trans. Geosci. Remote Sensing*, **37**(2), 1138-1150.

Dowling, R. D., and L. F. Radke, 1990: A summary of the physical properties of cirrus clouds. *J. Appl. Meteor.*, **29**, 970-978.

Heymsfield, A. J., 1972: Ice crystal terminal velocities. *J. Atmos. Sci.*, **29**, 1348-1357.

Heymsfield, A. J., K. M. Miller, and J. D. Spinhirne, 1990: The 27-28 October 1986 FIRE IFO cirrus case study: Cloud microstructure. *Mon. Wea. Rev.*, **118**, 2313-2328.

Kunz, K. S., and R. J. Luebbers, 1993: The Finite Difference Time Domain Method for Electromagnetics. CRC Press, Boca Raton, FL, 448 pp.

Matrosov, S. Y., 1991: Theoretical study of radar polarization parameters obtained from cirrus clouds. *J. Atmos. Sci.*, **48**, 1062-1069.

Mishchenko, M. I., J. W. Hovenier, and L. D. Travis, 1999:*Light Scattering by Nonspherical Particles.* Academic Press, San Diego, Chp. 6., 690 pp.

Taflove, A., 1995: "Computational Electrodynamics, The Finite-Difference Time-Domain Method." Artech House, Boston, MA.

Vivekanandan, J., V. N. Bringi, and R. Raghavan, 1990: Multiparameter radar modeling and observations of melting ice. *J. Atmos. Sci.*, **47**, 549-564.

Walsh, T. M., 1998: *Polarimetric scattering characteristics of planar and spatial ice crystals at millimeter wave frequencies.* PhD Thesis, The Penn. State Univ., 164 pp.

Walsh, T. M., and K. Aydin, 1999: 95 GHz reflectivity and difference reflectivity (Z_{DP}) signatures of pristine ice crystals in clouds. Preprints 29th Conf. Radar Meteor., Amer. Meteor. Soc., Montreal, Canada, 195-196.

Waterman, P. C., 1969: Scattering by dielectric obstacles. *Alta Freq.*, **38**, 348-352.

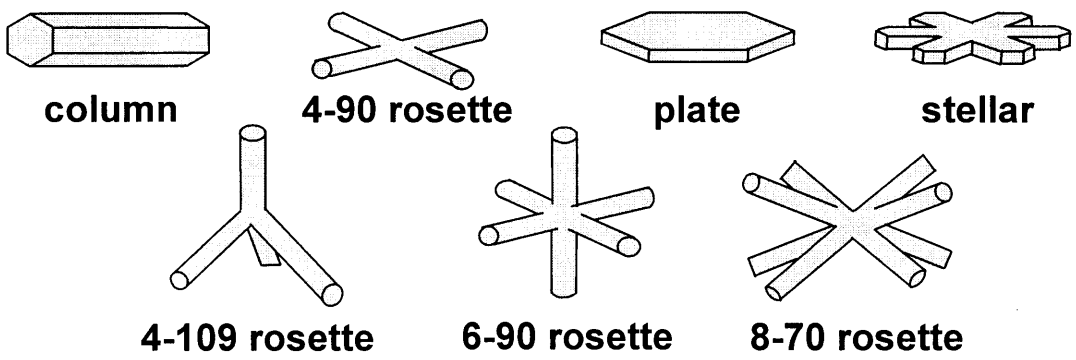

Fig. 1 Ice crystal models.

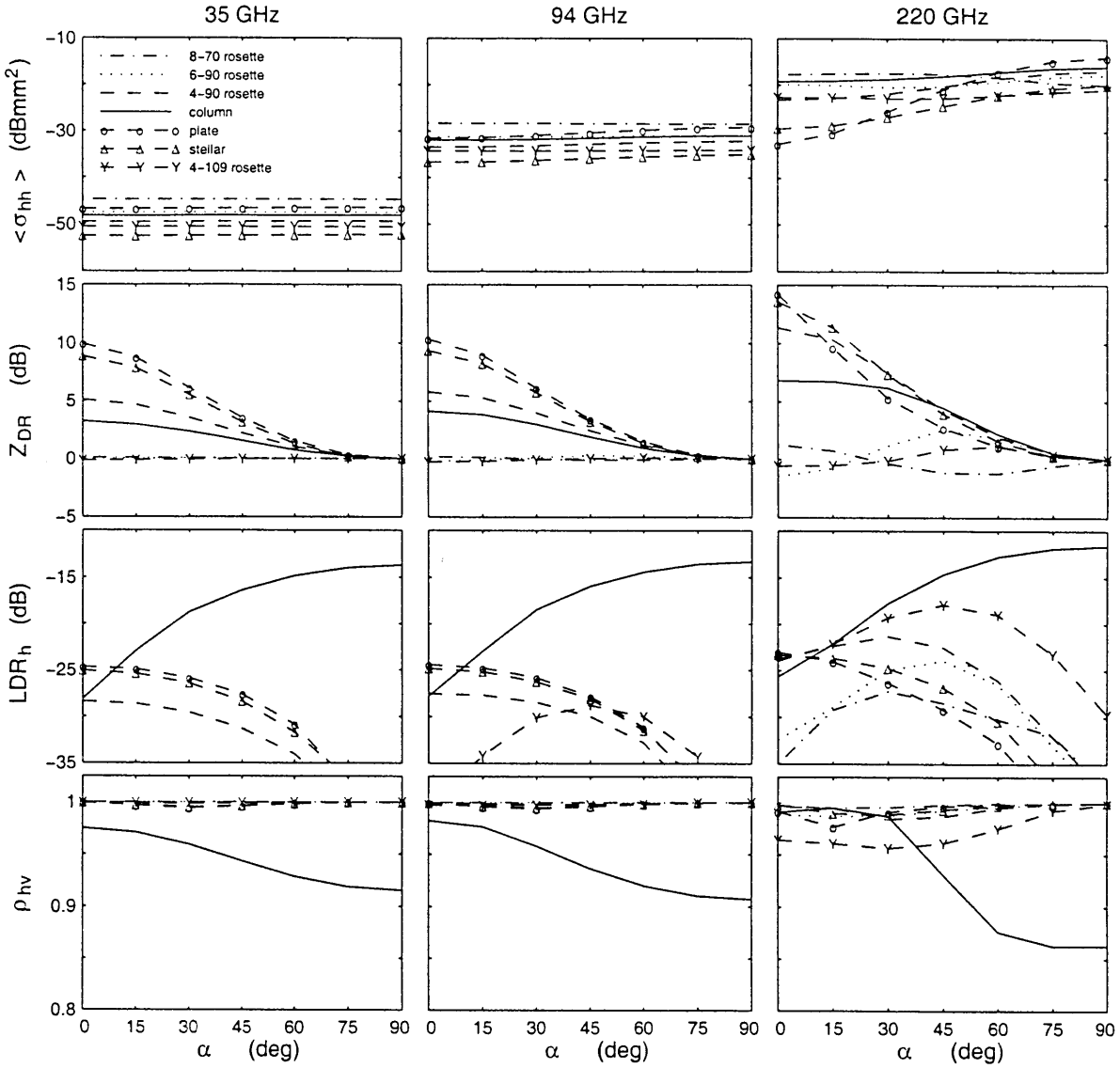

Fig. 2 Scattering parameters of ice crystals with a 0.8 mm maximum dimension D for the Gaussian canting angle model (see Section 2 for details) as a function of elevation angle α.

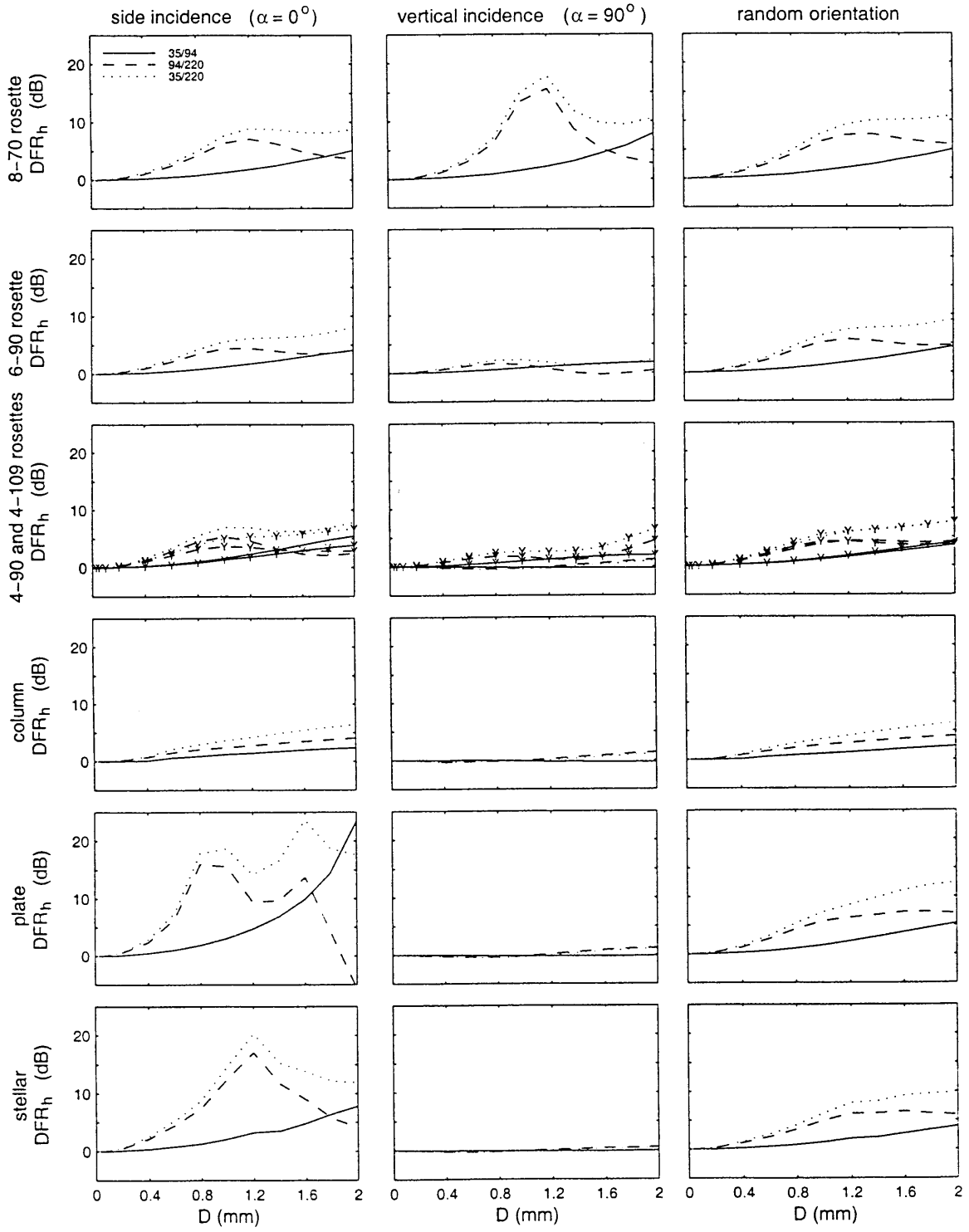

Fig. 3 Dual frequency ratios as a function of size D for the various crystal types. Side and vertical incidence models incorporate the Gaussian distribution for the canting angle with 5^0 standard deviation. The random orientation model. Incorporates a uniform (between 0^0 and 90^0) random distribution of the canting angle. The third row includes both the 4-90 and 4-109 (with the letter Y) rosettes. Adapted from Walsh (1998) and Aydin and Walsh (1999).

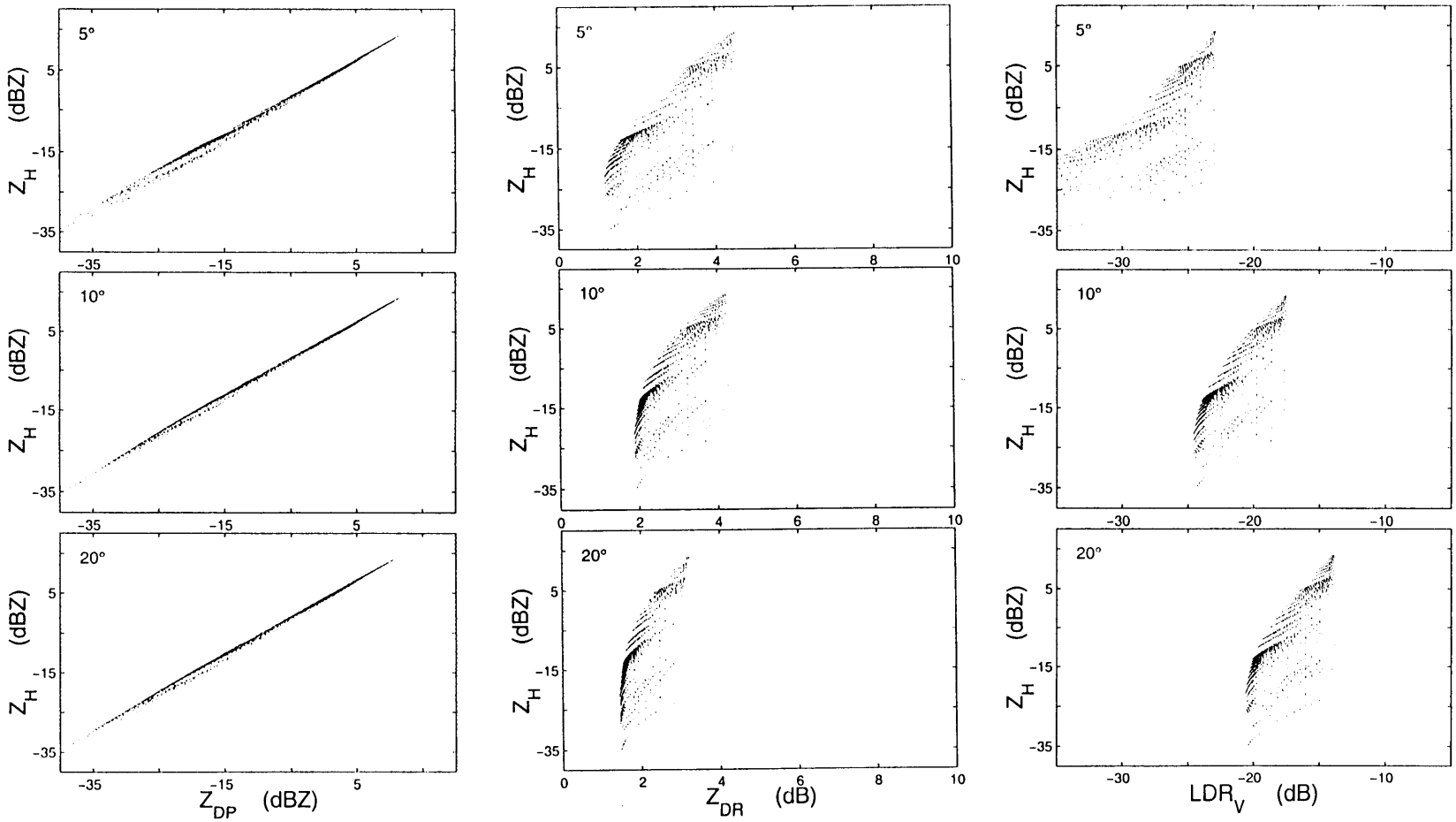

Fig. 4 Simulated radar observables for hexagonal columns at side incidence and 94 GHz for canting angle (see Section 2) with zero mean and standard deviation of 5^0, 10^0, and 20^0.

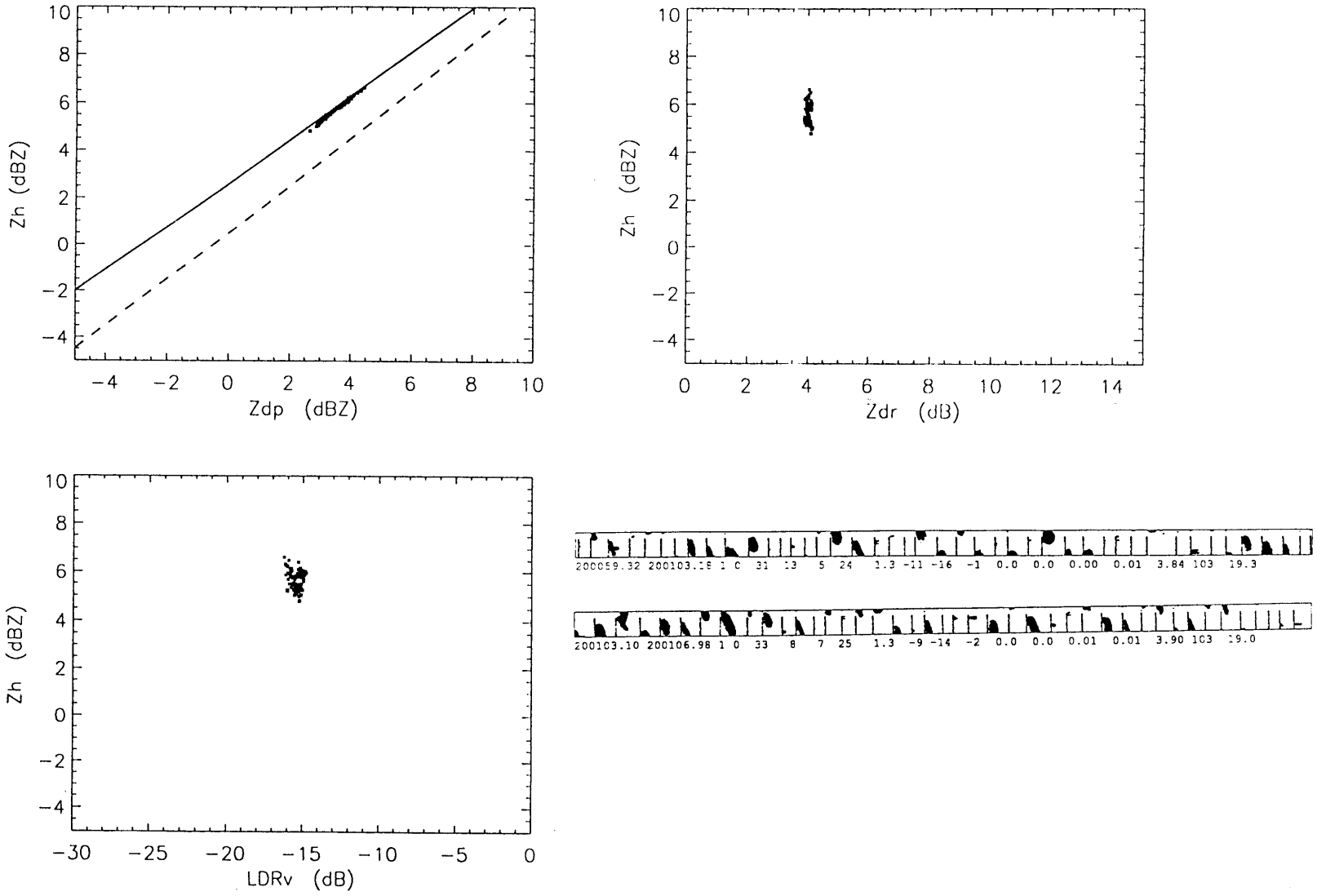

Fig. 5 Images from a 2D-C particle probe (maximum vertical dimension shown is 800 μm) and simultaneously obtained radar measurements (shown as dots in the three scatter plots) with the University of Wyoming's airborne 95 GHz radar system. The solid line in the $Z_h - Z_{DP}$ plane is the fitted curve to the simulations shown in Fig. 4 for hexagonal columns. The dashed line corresponds to stellar crystal model.